

# Brightness Fluctuations and Global Oscillations of the Sun (DIFOS Experiment)

Yu.D. Zhugzhda, V.D. Kuznetsov, and N.I. Lebedev

Helioseismology is the basic tool for the study of the solar interior, which is impossible to explore using the traditional optical methods. The solar interior is accessible to the modern helioseismic methods almost entirely except for the innermost regions of the solar core, where the helioseismology is perfectly complemented by the neutrino astronomy. The main product of helioseismic observations of the Sun is the solar eigenmode spectrum. At present, we can observe reliably the spectrum of acoustic-type oscillations with a period of  $\sim 5$  min called  $p$ -modes. The accuracy of determining the solar eigenmode frequencies depends on the signal-to-noise ratio and the duration of continuous observations. To ensure round-the-clock observations, networks of observing stations have been set up all round the world. Besides, space-born helioseismic experiments have been carried out. One of them was the DIFOS experiment on board the CORONAS-F spacecraft aimed at the observation of global oscillations of the Sun in the solar irradiance in the wavelength range from 350 to 1,500 nm. At present, data for a period of more than 10 years have been accumulated. However, the accuracy of a few thousandth of a  $\mu\text{Hz}$ , which corresponds to the 10-year observation period, was not achieved in determining the  $p$ -mode frequencies. This is because the  $p$ -mode spectral line is split into many components, which makes it difficult to determine the mean frequency. The complex structure of the spectrum is the result of stochastic excitation of oscillations.

## Continuous and Discrete Oscillation Spectra

When solar eigenmodes are observed by measuring the brightness or radial velocity fluctuations, the signal is always sampled. On one hand, this improves the

---

Yu.D. Zhugzhda (✉) · V.D. Kuznetsov · N.I. Lebedev  
Pushkov Institute of Terrestrial Magnetism, Ionosphere, and Radio Wave Propagation RAS  
(IZMIRAN), Troitsk, Moscow, Russia  
e-mail: [zhu@izmiran.ru](mailto:zhu@izmiran.ru)

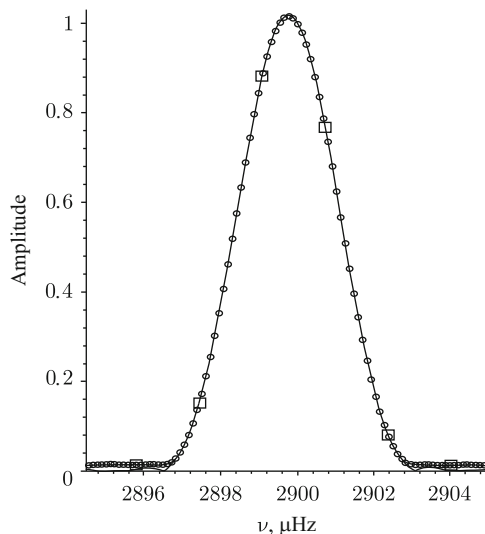


**Fig. 1** The spectral density of a model signal corrected for interruptions of observation due to the shadow entries of the satellite and telemetry problems is shown for three different processing methods. The *squares* indicate the discrete spectrum obtained using the fast Fourier transform; the *circles* show the discrete spectrum obtained likewise, but for a model signal, whose duration was increased by a factor of 14.5 by adding zero points; and the *solid line* indicates the continuous spectrum plotted with the use of the integral Fourier transform. From [14, p. 329]

signal-to-noise ratio through accumulation and, on the other hand, makes it possible to use the fast Fourier transform, thus reducing the data processing time. The discussion of this problem below is largely based on the material of paper [14].

In order to demonstrate the problems arising in the standard data processing method, let us first consider a model signal that reproduces in idealized form the actual observation data obtained during the CORONAS-F/DIFOS experiment, which are processed below. The model signal simulates observations for 7 days 50 min. The signal is interrupted every 94 min for about 40 min to imitate the shadow entries of the satellite. The interruptions due to the telemetry failures are also taken into account.

The sampling rate is 33.55 s. The squares in Fig. 1 indicate the discrete amplitude spectrum of the model signal obtained using the Hamming window, which is good at removing the effect of the realization ends. This is a typical situation where the true oscillation frequency falls somewhere in between the harmonics of the discrete spectrum, which makes it difficult to specify the true oscillation frequency. If instead of the model signal under consideration we take the corresponding analog continuous signal (even with the interruptions mentioned above), we can readily obtain the continuous spectrum using the integral Fourier transform. The continuous spectrum or, to be more precise, the spectral density is represented by the solid line in Fig. 1. For the continuous spectrum, the frequency of the spectral density maximum matches closely the frequency of the model signal.

In our case, it was easy to find the continuous spectrum, because we knew the continuous analog signal. The true spectrum of solar eigenmodes is difficult to determine, since the discrete spectrum recorded in the observations is used to obtain the discrete spectrum. This raises a natural question: How can the continuous spectrum of a signal be found from its values at discrete times? According to the Kotelnikov–Shannon theorem, a signal with the spectrum between the Nyquist frequency and the lowest frequency in the discrete spectrum can be fully restored from the values of the continuous signal at discrete times. The continuous signal  $s(t)$  can be restored from its values at times  $k \Delta t$  using the Kotelnikov–Shannon series:

$$s(t) = \sum_{k=-\infty}^{\infty} s(k \Delta t) \frac{\sin(t/\Delta t - k)}{t/\Delta t - k}. \quad (1)$$

As follows from this formula, an arbitrary continuous function  $s(t)$  can be represented without loss of information by a sequence of discrete values  $k \Delta t$ ,  $k = 0, 1, 2, \dots$  and can be unambiguously restored from this sequence if the highest frequency in spectrum of the function does not exceed its sampling frequency. This is the essence of the Kotelnikov–Shannon sampling theorem. Once the continuous signal corresponding to the discrete sequence is restored, its continuous spectrum can be found in principle by using the integral Fourier transform.

However, the integral Fourier transform for an actual signal is very difficult to perform. It takes much more computational time than obtaining the discrete spectrum by means of the fast Fourier transform. We are not aware of any attempts to restore the continuous analog signal and to obtain the continuous  $p$ -mode spectrum by using the scheme described above. Instead, the mean or maximum frequency of the  $p$ -mode lines in the solar eigenmode spectrum was found using various interpolations of the discrete spectrum based, for example, on the assumption of a Lorentz line profile.

It is quite clear that interpolation of the discrete spectrum cannot be used to find the spectral line profile without making additional assumptions, while passing to the continuous spectrum does not require additional hypothesis and is unambiguous. As a matter of fact, the continuous spectrum for a discrete signal can be readily found by a different method without passing to the analog signal via the Kotelnikov–Shannon series. Moreover, this can be done using the fast Fourier transform, which reduces the computational time essentially. The gradual passage from the discrete to continuous spectrum is performed through the increase of the realization length by adding points with zero signal values. When zeros are added, the number of harmonics in the spectrum increases. To eliminate the effect of decrease of the harmonic amplitude in the spectrum with increasing realization length  $T$ , the factor  $1/T$  must be excluded from the discrete Fourier transform. Besides, factor 2 must be taken into account, because, unlike the discrete spectrum, the continuous one contains only positive frequencies. Given these corrections, the spectral density will be determined using the fast Fourier transform. Note that

the increase of the realization length by adding zero points does not increase the frequency resolution; i.e., the spectrum width of the segment of a sine curve remains constant, while the number of harmonics in the spectrum increases.

The circles in Fig. 1 represent the discrete spectrum of our model signal extended in time by adding zero points up to the duration of 101 days and 19.38 h. One can see that the additional harmonics shown with the circles fall perfectly well on the profile of the continuous spectrum of the model signal, and the spectral line profile is well defined. Besides, it is evident from Fig. 1 that no increase of the realization length to infinity is required to find the continuous spectrum with a finite accuracy, but it will suffice to have a finite number of harmonics in the discrete spectrum. In principle, the continuous signal can also be restored if necessary using the inverse integral Fourier transform of the continuous signal found in this way. In the case of actual observations, this is absolutely unnecessary, since our goal is to study the individual  $p$ -modes that can be easily separated from the spectrum and only afterward can the inverse Fourier transform be applied to each of the modes separately. As a result, the analog signals will be isolated from the total signal for each of the oscillation modes of interest.

Below, the continuous spectrum will be used to construct the analytical signals for each of the oscillation modes. Thus, we pass to the continuous spectrum to be able to single out the continuous spectra for each of the oscillation modes present in the signal. By the way, the spectrum in Fig. 1, too, is only a part of the total spectrum of the model signal, which involves the side frequencies due to periodic interruptions of the signal when the satellite enters the Earth's shadow. Since the side harmonics are far enough from the central line, the spectrum of the "carrier frequency" can be isolated and studied separately. The inverse Fourier transform of the part of the total spectrum shown in Fig. 1 yields a continuous signal without interruptions due to the satellite shadow entries. This differs fundamentally from the restoration of the total signal including all  $p$ -modes and noise with the use of the Shannon–Kotelnikov series.

Of course, after the signal restoration according to the Shannon–Kotelnikov scheme and the subsequent determination of the continuous spectrum of the entire signal, one can, theoretically, also isolate individual spectral lines and find the continuous signal corresponding to each line by means of the inverse Fourier transform (Fourier inversion). However, this scheme for finding the continuous signal corresponding to an individual spectral line in the signal spectrum is very difficult to realize in practice. Our scheme, where the continuous spectrum is found by extending the realization through the addition of zeros, is very simple and does not take much computational time owing to the use of the fast Fourier transform.

Passing to the continuous spectrum makes the procedure of determining the maximum and mean spectrum frequency unambiguous and simple. As noted above, an assumption about the shape of the spectral line has to be made to find the spectral line maximum in the case of a discrete  $p$ -mode spectrum. For example, the hypothesis of Lorentzian shape is often used, though we are not quite sure that it is valid; moreover, the  $p$ -mode spectral lines were found to be asymmetric. Problems

associated with the use of the discrete spectrum arise when the line in the spectrum is at the resolution limit.

In this case, only a few harmonics of the discrete spectrum fall within the line band as shown for our model signal in Fig. 1. One would think that it will suffice to use a longer realization, which will ensure higher spectral resolution; i.e., more harmonics will fall within the line band. However, in the case under consideration, the lines of the  $p$ -modes split as the resolution increases, and each of the resulting components again is at the resolution limit; i.e., the same problem arises.

The model signal was constructed taking into account the interruptions in observation in order to find out how much the latter affect the oscillation spectrum. For this purpose, we constructed the second model signal of the same duration, but without interruptions. Its spectrum turned out to differ insignificantly from that of the signal with interruptions. The continuous spectrum of the second signal is also shown in Fig. 1. However, it is difficult to distinguish in the plot because of insignificant difference between both spectra with the exception of the line wings, which lie below and virtually coincide with the abscissa axis for the signal without interruptions.

## Analytical Signal and the Instantaneous Frequency

At first sight, the oscillation frequency, amplitude, and phase are trivial notions that do not require special explanation. Actually, however, they were much discussed mainly among radio physicists, since the demands of radio physics prompted a deep insight into the subject.

The frequency of oscillations, in particular, the  $p$ -mode frequency is usually thought of as the spectral frequency determined by the spectral analysis. However, besides the spectral frequency, there also exists the so-called instantaneous frequency, which is a function of time. It may be suggested that this is one of those frequencies that are determined by the wavelet analysis. But this is not the case, because the wavelet analysis determines the frequency of the wave trains of finite duration. The notions of the instantaneous frequency, amplitude, and phase of oscillations cannot be defined without introducing the so-called analytical signal. It is well known that, in the case of monochromatic oscillations, all calculations are simplified significantly by passing to a complex signal  $A \exp(i\omega t + \Phi)$ . The real part of the complex signal is the physical signal, which is observed, measured, and subjected to other procedures. A natural desire arises to use the complex signal in the case of non-monochromatic signal, too, especially as all actual physical signals are not monochromatic. The monochromatic signal is a convenient idealization that is used to simplify the theoretical analysis.

It has been established [2, 8, 9] that the only consistent method for passing from the real signal  $u(t)$  to the complex one  $\omega(t)$  is to introduce the so-called analytical signal, which can be obtained through the inverse Fourier transform of the continuous signal spectrum by the method described in the previous section.

The analytical signal is

$$w(t) = u(t) + i v(t) = A(t) e^{i \Phi(t)} \frac{1}{\pi} \int_0^{\infty} W(\omega) e^{i \omega t} d\omega, \quad \omega(t) = \frac{d\Phi(t)}{dt}, \quad (2)$$

where the imaginary and real parts of the analytical signal are related by the Hilbert transform:

$$v(t) = H(u(t)) = \frac{1}{\pi} \int_{-\infty}^{\infty} \frac{u(s) ds}{t - s}. \quad (3)$$

Here, the integration is performed according to the Cauchy principal value;  $A(t)$ ,  $F(t)$ , and  $w(t)$  are the instantaneous amplitude, phase, and frequency of oscillations; and  $W(\omega)$  is the spectral density. The analytical signal was first defined by Gabor [4]. The use of the analytical signal runs into certain difficulties [2, 8, 9] when broadband signals and fast amplitude variations are dealt with. But in the case of  $p$ -modes, no difficulties arise, since their bandwidth is small compared to their frequency, and the timescale of their amplitude variations is longer than the period by many orders of magnitude. To find the analytical signal of an individual oscillation mode, the integration in (3) is performed only within the frequency range that involves the selected spectral line. For our model signal, the integral was taken within the range indicated in Fig. 1.

Passing to the analytical signal, we shall be able to study the time evolution of the signal amplitude and frequency separately. Obviously, the instantaneous and spectral frequencies differ. Only their mean values  $\overline{\omega(t)}$  and  $\tilde{\omega}$  obtained by the time and spectral averaging are equal. The averaging is performed as follows:

$$\overline{\omega(t)} = \frac{\int_{-\infty}^{\infty} \omega(t) A(t)^2 dt}{\int_{-\infty}^{\infty} A(t)^2 dt} = \frac{\int_{-\infty}^{\infty} \omega |W(\omega)|^2 d\omega}{\int_{-\infty}^{\infty} |W(\omega)|^2 d\omega} = \tilde{\omega}. \quad (4)$$

Besides, there is a very important relationship between the second moments of the instantaneous and spectral frequency that is reduced to:

$$\begin{aligned} \overline{\omega(t)^2} + \overline{\left(\frac{dA(t)}{dt}\right)^2} &= \frac{\int_{-\infty}^{\infty} \omega(t)^2 A(t)^2 dt}{\int_{-\infty}^{\infty} A(t)^2 dt} + \frac{\int_{-\infty}^{\infty} \left(\frac{dA(t)}{dt}\right)^2 dt}{\int_{-\infty}^{\infty} A(t)^2 dt} \\ &= \frac{\int_0^{\infty} \omega^2 |W(\omega)|^2 d\omega}{\int_0^{\infty} |W(\omega)|^2 d\omega} = \tilde{\omega}^2. \end{aligned} \quad (5)$$

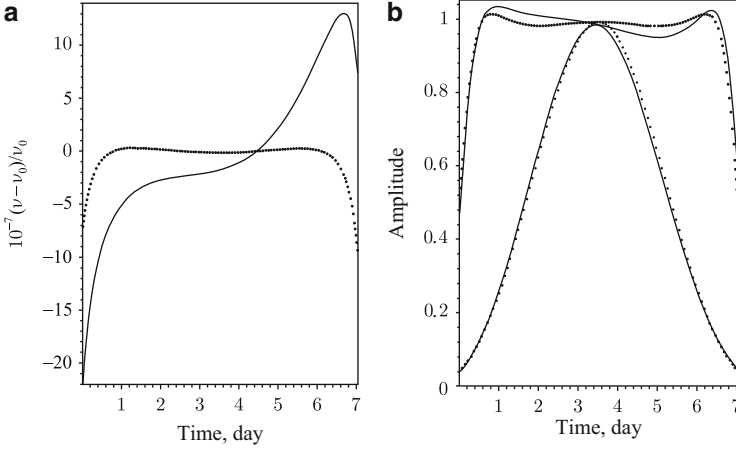


**Fig. 2** Relative variations of the instantaneous frequency (a) and amplitude (b) as a function of time for the continuous (*dotted curve*) and discontinuous (*solid curve*) model signals. The right-hand panel shows also the time dependence of the instantaneous amplitude of the two model signals corrected for the Hamming window function (7). In the latter case, the amplitude changes insignificantly, except for the ends of the time interval. From [14, p. 329]

As follows from this formula, the relationship between the deviations  $(\delta\omega)^2$  and  $(\Delta\omega)^2$  of the instantaneous and spectral frequency is:

$$\begin{aligned} (\delta\omega)^2 &= \overline{\omega(t)^2} - (\overline{\omega(t)})^2, \quad (\Delta\omega)^2 = \widetilde{\omega^2} - (\widetilde{\omega})^2, \\ (\Delta\omega)^2 &= (\delta\omega)^2 + \overline{\left(\frac{dA(t)}{dt}\right)^2}. \end{aligned} \quad (6)$$

This formula reflects the important physical fact that the effective spectral width determined by the deviation of the spectral frequency is the sum of the broadenings caused by the frequency and amplitude modulations, which are equal, respectively, to the instantaneous frequency deviation and r.m.s. fluctuation of the time derivative of the instantaneous signal amplitude.

Thus, the introduction of the analytical signal allows us to separate two effects that influence the spectral width. The formulas given above were first derived by Fink [2, 3] for an analytical signal. It should be noted, however, that, long before Gabor [4] introduced the analytical signal, the same formulas had been derived by Rytov [6] for periodic signals.

Figure 2 shows the instantaneous frequency and amplitude of two model signals described in the previous section. The relative (with respect to the exact frequency  $\nu = 2899.775626 \mu\text{Hz}$ ) variations of the instantaneous frequency of the continuous model signal proved to be of the order of or smaller than  $3 \cdot 10^{-8}$  outside the zones of influence of the realization ends. The Hamming window used to analyze both model

signals is rather efficient still it does not fully suppress the Gibbs effect, which gives rise to spurious fluctuations of the instantaneous frequency and amplitude.

The somewhat stronger fluctuations of the instantaneous frequency of the discontinuous model signal (solid curve in Fig. 2a) occur, probably, as a result of the Gibbs effect due to the presence of unsmoothed interruption ends in the signal that simulates the interruption in the DIFOS photometric observations because of the telemetry failure in the second half of the observation period. This interruption also manifests itself in the time dependence of the amplitude of the discontinuous model signal. This becomes obvious only after the amplitude dependence has been corrected by division by the Hamming window function, which equals to

$$H(t) = 0.54 - 0.46 \cos\left(\frac{2\pi t}{T}\right), \quad (7)$$

where  $T$  is the realization length.

As seen in Fig. 2b, the amplitude of the interrupted signal corrected by the Hamming window function has a minimum in the second half of the interval. It should be noted that the amplitude by no means drops to zero as might be expected. This is because, actually, the instantaneous amplitude and frequency are not instantaneous, but are rather the means for a certain time interval. The Gibbs effect might, probably, be reduced by smoothing the ends of long interruptions in observations; however, we did not do it, since the accuracy achieved in reproducing the constant instantaneous frequency of the model signal proved to be very high. This manifests itself particularly clearly in the relative accuracy of the mean instantaneous frequencies  $(\overline{\nu(t)} - \nu_0)/\nu_0$ , which are, respectively,  $-1.06 \cdot 10^{-7}$  and  $-1.03 \cdot 10^{-9}$  for the continuous and interrupted signal; i.e., the mean instantaneous frequency is somewhat smaller than the true frequency of the periodic signal used to construct the model signals. Thus, the accuracy of the signal frequency was extremely high. This justifies the use of the method of analytical signal for the analysis of actual observations. The deviation of the instantaneous frequency  $\delta\nu$  of both signals was zero. This suggests that using the analytical signal allowed us to establish that both model signals are exactly harmonic, which could not be established using the ordinary harmonic analysis of the signal.

Thus, introducing the Hamming window resulted in an insignificant shift of the mean frequency and did not lead to a broadening of the signal spectrum due to the spurious modulation caused by the Gibbs effect. Consequently, the analysis of the instantaneous frequency deviation shows that the spectral line width of the model signal is determined only by amplitude fluctuations. This agrees with the fact, since the model signals are segments of a sine wave. The use of the Hamming window introduces an additional amplitude modulation, which leads to a broadening of the spectrum: the widths of the spectra calculated with the analytical signal are 1.714 and 1.722  $\mu\text{Hz}$  for the continuous and interrupted model signals, respectively. The spectrum width of both model signals found by calculating the second moment of the continuous spectrum turned is 1.726  $\mu\text{Hz}$ ; i.e., equality (5) holds to within the third decimal place. The correction of the analytical signal amplitude through



division by the function  $H(t)$  reduced the spectrum widths of the two model signals to 1.458 and 1.442  $\mu\text{Hz}$ , respectively, owing to the decrease of the signal amplitude fluctuations. The suggested amplitude correction does not cause undesirable effects, such as the Gibbs effect, which restricts significantly the capabilities of the spectral analysis.

In the next section, the analytical signal is used to analyze the observations of  $p$ -modes within the frames of the CORONAS-F/DIFOS experiment.

## Observation of the Solar Brightness Fluctuations

The DIFOS experiment on board the CORONAS-F satellite [5] was designed to observe the global oscillations of the Sun and to study its interior structure. The observations were made with a multi-channel photometer, DIFOS, which measured the intensity fluctuations of the solar radiation from the ultraviolet to near infrared range simultaneously in six optical bands. Two measuring channels (for 650 and 850 nm) were dubbed to estimate the proper noise contribution of the device. Figure 3 illustrates the functional diagram of the DIFOS photometer. Only three of the eight spectral measuring channels are represented for simplicity.

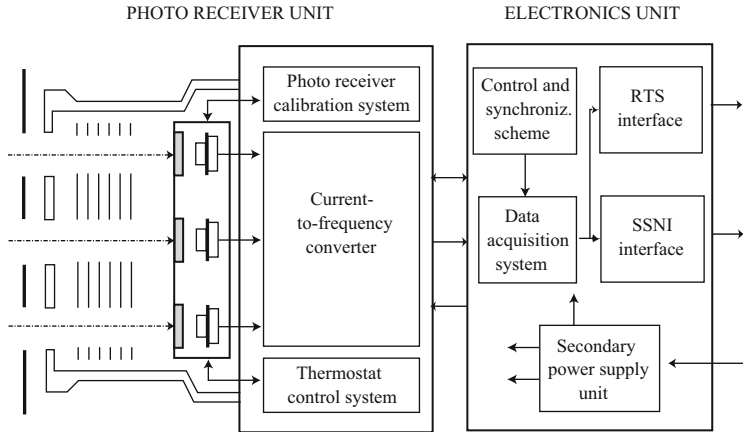
The CORONAS-F/DIFOS photometer was measuring the emission intensity simultaneously in six spectral channels: 350, 500, 650, 850, 1,100, and 1,500 nm with a bandwidth of 10 % of the central frequency covering a broad spectral range from the near ultraviolet to infrared radiation.

The relative intensity resolution of the photometer was  $2 \cdot 10^{-6}$  of the total solar irradiance; the intensity sampling rate was 33.554 s; the spatial resolution was absent (accessible to observation were the lower-order oscillation modes with  $l \leq 3$ ); the field of view of the photometer was  $2^\circ$ ; the orientation of the photometer optical axis to the center of the Sun was no worse than  $10'$  (controlled by the satellite navigation system).

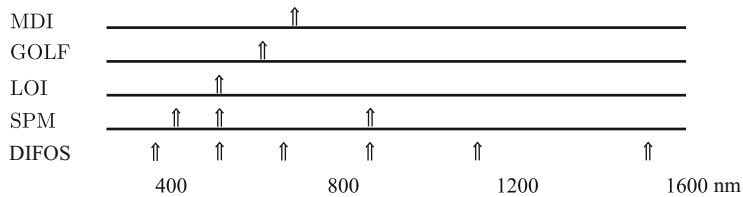
The CORONAS-F satellite was launched on 31 July 2001 to the high-latitude ( $82.5^\circ$ ) circular orbit at a height of about 500 km. The DIFOS photometer was brought into operation on 15 August 2001 and was functioning without interruption until the end of the CORONAS-F mission on 3 December 2005. During this period, the solar radiation intensity was measured in the vicinity of and after the maximum of Cycle 23. The total length of the records obtained amounts to 4 years, 3 months, and 11 days.

Figure 4 shows the relative position of the spectral channels of the CORONAS-F/DIFOS photometer and the SOHO instruments.

The DIFOS photometer started measurements on 22 August 2001. The data on radiation intensity were transmitted from the satellite via two independent telemetry systems. This allowed us to restore by comparison the data lost as a result of the failure in one of the systems. The analysis showed a good quality of the data obtained. The losses did not exceed 10 % of the photometer operation time and were associated mainly with the quality of reception of the telemetry at the receiving points.



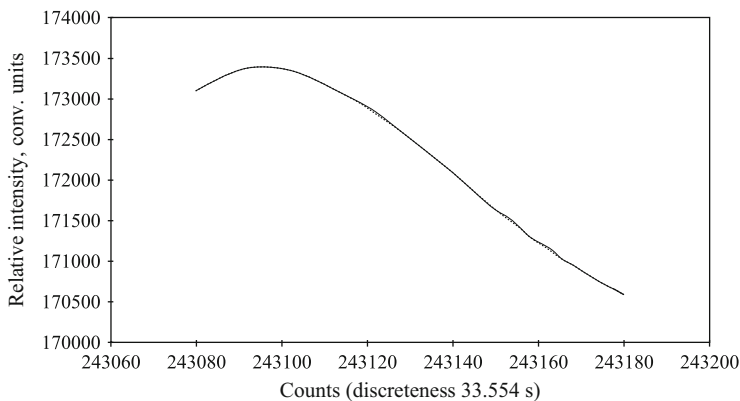
**Fig. 3** The functional diagram of the multi-channel photometer. From [5, pp. 871–875]



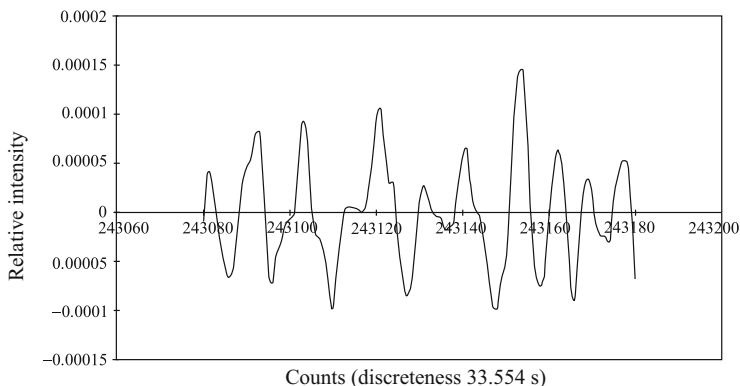
**Fig. 4** The relative position of the spectral channels of the DIFOS photometer and the SOHO helioseismic instruments (*MDI* Michelson Doppler Imaging of solar oscillations, *GOLF* Global low-degree velocity, *LOI* Luminosity Oscillation Imager, and *SPM* SunPhotoMeter). From [5, pp. 871–875]

Figure 5 represents a record obtained in one of the photometer measuring channels along the sunlit part of the satellite trajectory. The trend observed is attributed to the scattering of light reflected from the Earth surface that gets inside the instrument. The figure shows the analytical curve that approximates the trend.

After cleaning the record shown in Fig. 5 (subtracting the photo receiver dark currents and trends, normalizing, etc.), we obtained the variation of the solar emission intensity represented in Fig. 6. The intensity variation in this figure does not exceed 0.02 % of the total flux. The time series of the required length composed of such one-rotation records was used to obtain the amplitude spectra in the spectral range of 0–5  $\mu\text{Hz}$ .



**Fig. 5** The intensity of solar radiation as measured in the 350 nm channel along the sunlit part of the satellite trajectory. The trend is due to the light scattered and reflected from the Earth's atmosphere. The analytical fitting curve is presented. From [5, pp. 871–875]



**Fig. 6** Variations of the solar emission intensity as measured in the 350 nm channel. From [5, pp. 871–875]

## The Instantaneous Amplitude, Frequency, and Phase of $p$ -Modes at Various Levels in the Photosphere

The analytical signal method was used to analyze the solar brightness fluctuations observed within the frames of the CORONAS-F/DIFOS experiment.

The eight-channel photometer, DIFOS, was designed to observe the Sun as a star in six optical bands, namely, 350, 500, 650, 850, 1,100, and 1,500 nm. DIFOS had two independent photometers in each of the 650 and 850-nm bands, which enabled us to estimate the noise by comparing the signals in the parallel channels.

The data from the 1,100-nm channel will not be used because, unfortunately, they contain much noise, which is, apparently, due to the glare associated with reflections from the surrounding equipment.

The series of observations used for the analysis is a bit longer than a week, which is very short by today's standards. Nevertheless, it was not only sufficient to demonstrate the efficiency of the method based on the use of an analytical signal, but also provided some new results essential to helioseismology. Two modes with  $l = 0$  and  $n = 20, 21$  were chosen for the analysis. The modes with  $l = 0$  were taken because they are not subject to splitting due to the solar rotation, which complicates the analysis significantly. The analytical signal for the chosen realization was constructed by exactly the same method as that used for the model signal with interruptions considered above.

Figure 7 illustrates the time dependence of the instantaneous amplitude. The instantaneous amplitude is corrected for the Hamming window. The amplitude variations differ in character for the two chosen modes. The amplitude for the  $n = 20$  mode changes more smoothly than that for  $n = 21$ . The time variations of the instantaneous frequency of both modes also differ essentially. Compared to a smooth frequency variation of the  $n = 20$  mode, the  $n = 21$  mode displays narrow peaks of the instantaneous frequency. Particularly prominent are the instantaneous frequency maxima recorded in the 1,500-nm channel, which measures emission from the deepest photospheric layers. The maxima of the instantaneous frequency correspond to the minima of the instantaneous amplitude. This is particularly well pronounced in the 1,500-nm channel, whose amplitude is smaller than that of the other channels and is located in the lowest part of Fig. 7. The variations in the phase shift also correlate closely with the instantaneous frequency fluctuations: the phase variations are fastest at the instantaneous frequency maxima. It seems that the instantaneous frequency of the  $n = 20$  mode also tends to reach the maximum immediately outside the time interval under examination; however, one cannot rule out that this is merely the effect of the realization ends. On the whole, the behavior of the analytical signal for the two chosen modes is different.

Figure 8 represents the results of calculation of the mean oscillation frequencies, dispersions, and phase shifts using both the oscillation spectra and the analytical signal. The left column illustrates the oscillation phase shifts with respect to the 1,500 nm channel. The phase shift between the channels was determined by two methods. The circles in Fig. 8 show the phase shifts determined from the spectra constructed for each channel. The phase shifts for the parallel channels do not always coincide perfectly. This can be attributed to the influence of noise or scattered light, which may differ in the parallel channels. The lines in Fig. 8 were plotted using the mean values in the parallel channels. The phases were also determined by time averaging of the phase difference between the analytical signals of the channels. In this case, the phase differences in the parallel channels did not always coincide either.

The phase differences determined by two methods proved to agree perfectly well. They clearly revealed the delay of oscillations in the 500-nm channel relative to

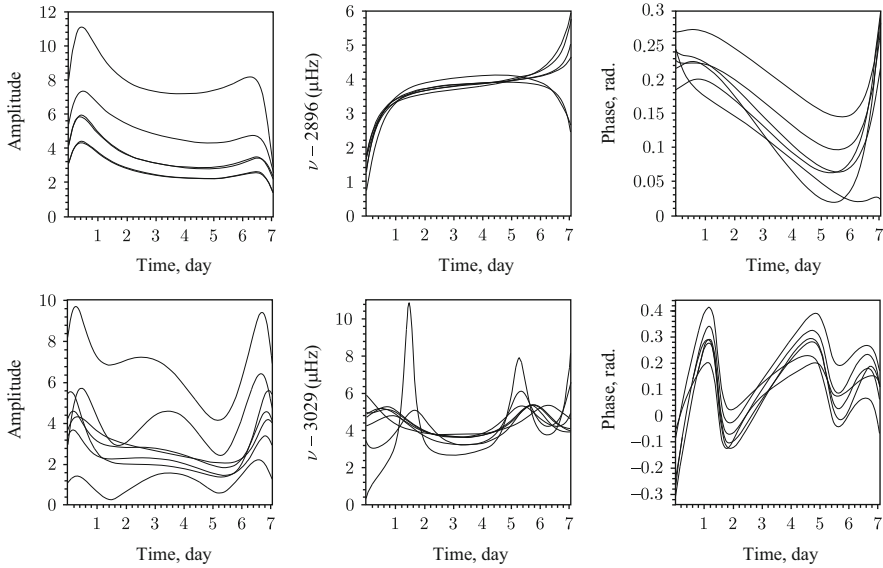


**Fig. 7** The instantaneous amplitude (in units  $10^{-5}$  of the mean solar flux in the corresponding photometer channel), the excess of the instantaneous frequency ( $\mu\text{Hz}$ ) above 2,896 and 3,029, and the phase shifts (rad) in the optical channels of 350, 500, 650, and 850 nm relative to the 1,500-nm channel. The *upper* row of plots was constructed for the mode with  $l = 0, n = 20$  and the *lower* one, for  $l = 0, n = 21$ . From [14, p. 329]

those in the 350- and 1,500-nm channels by  $\sim 30$  s, which corresponds to the phase velocities of  $\sim 3$  km/s.

The emissions at 350 and 1,500 nm come, respectively, from the uppermost and the deepest photospheric layers, while the emissions at 500, 650, and 850 nm originate in the middle photosphere. Hence, the waves from the upper and lower layers travel to the middle photosphere. A seemingly odd behavior of the waves can be naturally explained in terms of the nonadiabatic wave theory, which we shall consider in detail when discussing our results.

The middle column in Fig. 8 presents the frequencies of the two chosen modes determined both directly from the continuous spectrum and by averaging the instantaneous frequency. The frequencies obtained by two different methods differ. Being insignificant for the  $n = 20$  mode, this difference can no longer be attributed to inaccurate calculation for the  $n = 21$  mode. This is because the signal is not a single-component one as will be shown in the following section. Anticipating that discussion, we should emphasize that equality (4) is only valid for a single-component signal, i.e., for a quasi-monochromatic signal with smoothly varying frequency and amplitude.

It should also be noted that the  $p$ -mode frequencies change from channel to channel. The knowledge of the cause of this variation is essential to helioseismology, since the main objective of the latter is to determine the solar eigenmode spectrum

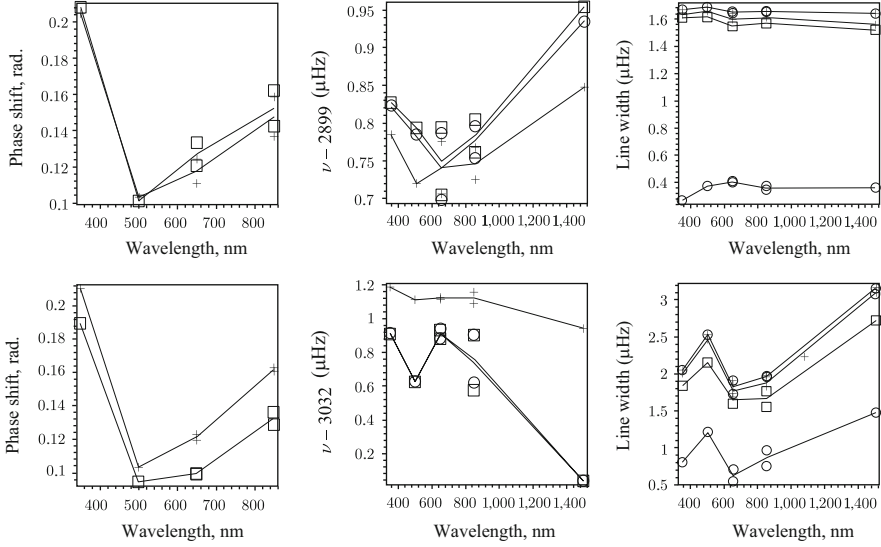


**Fig. 8** Mean parameters of the  $l = 0, n = 20$  (upper row) and  $l = 0, n = 21$  (lower row) modes. The *left column* represents the phase differences between the 350, 500, 650, and 850-nm channels and the 1,500-nm channel. The *squares* denote the differences of the time-averaged instantaneous phases  $\overline{\Phi(t)}$ . The *crosses* show the phase differences at the maxima of the continuous spectra in the corresponding channels. The *middle column* represents the mean instantaneous frequency  $\omega(t)$  (*squares*) and spectrum-averaged frequency  $\bar{\omega}$  (*crosses*). The *circles* denote the frequencies at the maxima of the continuous spectra in the corresponding channels. The *right column* represents the full line widths determined directly from the spectrum (*circles*) and by using the analytical signal (*crosses*), as well as the contribution to the full line width from the amplitude (*squares*) and frequency (*circled crosses*) modulation. From [14, p. 329]

as accurate as possible. Generally speaking, the instantaneous frequency of a signal can change when passing through linear systems, while the spectral frequency must remain constant.

The true spectral frequency can only be found by averaging over a sufficiently long time interval. In other words, averaging over a short time interval will yield but a smoothed instantaneous frequency. How long the averaging interval must be for obtaining the spectral frequency depends on the stability of the signal. We shall return to this question when discussing the observation results. Note, however, that the useful signal can be affected by various noise components, including those of solar origin. The first thing that calls our attention is a significant difference between the properties of the  $n = 20$  and  $n = 21$  modes as we noted above when analyzing the behavior of the instantaneous frequencies and amplitudes of oscillations. The range of channel-to-channel variations of the mean frequencies is much larger for the  $n = 21$  mode. As shown in the next section, this is due to the presence of a signal close in frequency.

The right column in Fig. 8 shows the full line widths obtained both directly from the spectrum and with the use of the analytical signal, as well as the contribution to the spectrum width from the frequency and amplitude fluctuations. The full spectral widths determined by both methods virtually coincide as they should do according to the theory (5). The contributions to the line width from the amplitude and frequency fluctuations cannot be separated unless we use the analytical signal (5). Again, an essential difference can be noted between the parameters of the two modes.

The spectral width for the  $n = 20$  mode is at the resolution limit depending on the realization length and does not virtually change throughout the photosphere, which is covered completely owing to the choice of frequencies of the optical channels. The line width is determined, primarily, by the amplitude modulation, while the contribution of the frequency modulation is insignificant. The spectral width for the  $n = 21$  mode is much larger, although the contribution of the frequency modulation is also small. An important factor is that the spectral width is determined by the amplitude modulation rather than the realization length as is, apparently, the case for the  $n = 20$  mode.

Indeed, in the latter case, the difference between the line widths determined by two different methods, as well as the width values themselves differ little from those found above for the model signals. This implies that the  $n = 20$  line width may be even smaller, which can be revealed if longer observation series are processed. The analysis of the  $n = 21$  mode will be continued in the next section where we shall propose another method for studying oscillations based on the analytical signal.

The relationship between the effects of amplitude and frequency fluctuations is of particular interest in the context of determining precise  $p$ -mode frequencies. At present, it is believed that the full line width is the measure of accuracy of the oscillation frequency. This follows from the assurance that the amplitude and frequency fluctuation effects responsible for the  $p$ -mode line broadening are impossible to separate.

True enough, these effects cannot be separated using the classical spectral methods. Actually, it is not the full line width  $(\Delta\omega)^2$  but the instantaneous frequency deviation  $(\delta\omega)^2$  resulting only from the frequency fluctuations that must be considered the true accuracy measure of the oscillation frequency. This obvious fact is not questioned, for example, when the methods for measuring the frequency of quantum frequency standards are developed. However, when applied to the results of our analysis, this approach runs into some fundamental difficulties associated with rather small frequency fluctuations of the  $p$ -modes under examination. For example, if the spectral line width for the  $n = 20$  mode were determined by the frequency fluctuations alone, it would not exceed  $0.4 \mu\text{Hz}$ . This value is much smaller than the uncertainty in the frequency determination,  $1.65 \mu\text{Hz}$ , which follows from the uncertainty relation  $\Delta\omega \Delta t \leq 1$ .

On the other hand, with the model signal as an example, we could make sure that the accuracy of determining the frequency using the analytical signal is actually limited by the accuracy of our calculations. At the same time, the frequency of the maximum of the continuous spectrum of the model signal also coincides with

the frequency of the model signal within the calculation accuracy. Likewise, the frequencies of the spectral maxima and the mean instantaneous frequencies of both modes under discussion are very close in all optical bands as is readily seen in Fig. 8 (middle column). However, it also follows from Fig. 8 that the difference between the spectrum-averaged frequencies and the time-averaged instantaneous frequencies is much larger because of the amplitude modulation.

We believe that the goal of the helioseismology must be determining the mean instantaneous frequency over long time intervals. These mean frequencies must, in principle, coincide with the frequencies of the maxima of spectral lines in the continuous spectrum. However, as noted above, the latter are difficult to determine because of the jaggedness of spectral lines in the spectra obtained by long-term observations. We hope that the use of the analytical signal will help us overcome this difficulty. An important advantage of using an analytical signal is the possibility to determine the instantaneous frequency deviation, which is the measure of stability and accuracy of the solar eigenmode frequency. It is to be emphasized that the reasoning above suggests implicitly that the signal under examination is monochromatic. Of course, this assumption is not always valid. In the next section, we show that using an analytical signal helps us overcome this difficulty in the data analysis.

## The Analytical Signal and Separation of a Two-Component Signal

In numerous applications of the method of analytical signal (the analysis of radio engineering circuits, nonlinear oscillations, random processes, parametric oscillations, etc.), it is always emphasized that the method is suitable, primarily, for the study of narrow-band monochromatic signals. The effects related to the influence of various types of noise were also considered, but it was specially noted that the presence of other narrow-band signals involves serious problems making the use of the analytical signal inefficient [1, 6].

Let us show that this opinion is erroneous, and the use of an analytical signal is quite efficient in the particular case of a two-component signal. This approach can also be applied to a three-component signal.

Let us consider the simplest two-component real signal

$$u(t) = A_1 \cos(\omega_1 t + \varphi_1) + A_2 \cos(\omega_2 t + \varphi_2), \quad \omega_{1,2} = 2\pi \nu_{1,2},$$

$$A_1, A_2 > 0, \quad \omega_1 > \omega_2. \quad (8)$$

The imaginary part of the analytical signal for this real signal is

$$v(t) = A_1 \sin(\omega_1 t + \varphi_1) + A_2 \sin(\omega_2 t + \varphi_2), \quad (9)$$



and its instantaneous frequency and squared instantaneous amplitude are, respectively,

$$\omega(t) = \frac{A_1^2 \omega_1 + A_2^2 \omega_2 + 2A_1 A_2 (\omega_1 + \omega_2) \cos((\omega_1 - \omega_2)t + \varphi_1 - \varphi_2)}{A^2(t)}, \quad (10)$$

$$A^2(t) = A_1^2 + A_2^2 + 2A_1 A_2 \cos((\omega_1 - \omega_2)t + \varphi_1 - \varphi_2). \quad (11)$$

The amplitude and frequency of the analytical signal are periodic functions with a period  $T = 2\pi/(\omega_1 - \omega_2) = 1/(\nu_1 - \nu_2)$ .

The frequency and amplitude extrema of the analytical signal occur at the times

$$T_{\text{ext}} = (n - \Delta\varphi)T, \quad n = 0, 1, 2, \dots, \quad \Delta\varphi = \varphi_1 - \varphi_2 \text{ (rad)}, \quad (12)$$

and the frequency and amplitude values at the extremum are, respectively

$$\nu_{\max 1} = \frac{A_1 \nu_1 + A_2 \nu_2}{A_1 + A_2}, \quad \nu_{\max 2} = \left| \frac{A_1 - \nu_1 - A_2 \nu_2}{A_1 - A_2} \right|, \quad (13)$$

$$A_{\max 1} = A_1 + A_2, \quad A_{\max 2} = |A_1 - A_2|. \quad (14)$$

If the instantaneous frequency at its extrema and the distance  $T$  between its maxima or minima are known, then the harmonic frequencies of the two-component signal can be derived from the above formulas:

$$\begin{aligned} \nu_2^{(1,2)} &= \frac{1}{2} \left( \nu_{\max 1} + \nu_{\max 2} - \frac{1}{T} + \sqrt{(\nu_{\max 1} - \nu_{\max 2})^2 + \frac{1}{T^2}} \right), \\ \nu_1^{(1,2)} &= \nu_2^{(1,2)} + \frac{1}{T}. \end{aligned} \quad (15)$$

Naturally, the harmonic frequencies of the signal do not depend on the amplitudes of the constituent harmonics. The first pair of frequencies  $\nu_1^{(1)}$ ,  $\nu_2^{(1)}$  corresponds to the case when the higher-frequency harmonic has smaller amplitude. In this case, the minima of the instantaneous frequency are sharper than the maxima. The other pair of frequencies corresponds to the case when the amplitude of the higher-frequency harmonic exceeds that of the lower-frequency one. In this case, the maxima of the instantaneous frequency are sharper than the minima as shown in Fig. 9 analyzed below.

Knowing only  $\nu_{\max 1}$ ,  $\nu_{\max 2}$ , and  $T$ , we can obtain the harmonic amplitude ratio

$$\frac{A_1}{A_2} = \left| \frac{\nu_{\max 1} - \nu_2}{\nu_{\max 1} - \nu_1} \right| = \left| \frac{\nu_{\max 2} - \nu_2}{\nu_{\max 2} - \nu_1} \right|. \quad (16)$$

In order to find the absolute values of the constituent harmonic amplitudes of a two-component signal, it is necessary to determine additionally the variation range of the

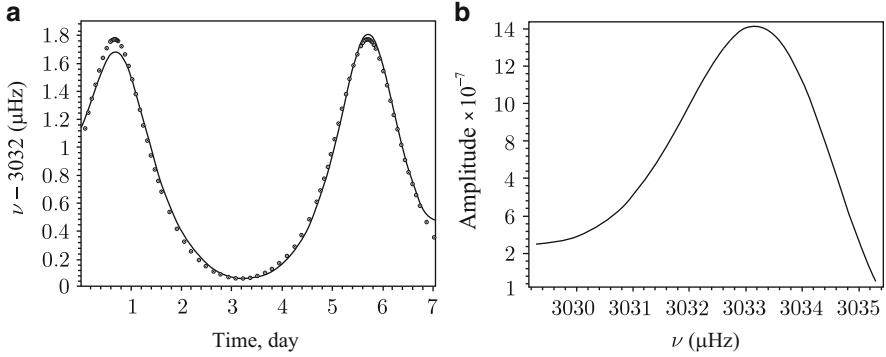


**Fig. 9** The instantaneous frequency vs. time (panel **a**, solid line) and the oscillation spectrum (panel **b**) in one of the 850 nm channels. The dotted line shows the calculated instantaneous frequency. From [14, p. 329]

instantaneous amplitude  $A_{\max 1} - A_{\max 2}$ , which is twice the amplitude of the smaller harmonics

$$|A_1 - A_2| = 2 \min(A_1, A_2). \quad (17)$$

Figure 9a illustrates the time dependence of the instantaneous frequency for the  $n = 21$  mode in one of the 850 nm channels of the DIFOS photometer. The same picture represents the instantaneous frequency calculated for a two-component signal with the frequencies  $\nu_1 = 3033.23 \mu\text{Hz}$  and  $\nu_2 = 3030.93 \mu\text{Hz}$  and the harmonic amplitude ratio  $A_1/A_2 = 3.02$ . The harmonic frequencies and their ratio were found from (15) and (16), and the maxima of the observed and calculated signals were matched by choosing the phase  $\varphi_1 - \varphi_2$ , whose variation makes the instantaneous frequency maxima shift along the time axis. The coincidence of the observed and calculated signals is nearly perfect. Thus, it can be established reliably that, apart from the principal harmonic, the signal contains a second harmonic with an amplitude three times smaller than that of the principal harmonic and a frequency differing by only  $2.3 \mu\text{Hz}$ .

In order to demonstrate an exceptional sensitivity of the instantaneous frequency to the presence of additional signal components, Fig. 9 (right-hand panel) shows the spectrum of the  $n = 21$  mode for the 850 nm channel. It is clear that not only is such a weak additional component in the spectrum of the  $n = 21$  mode impossible to isolate by any methods of the classical spectral analysis, but one cannot assert with confidence that the oscillation consists of two harmonics rather than being a single mode with an asymmetric spectrum. The signal separation into harmonics with the aid of an analytical signal is very efficient and allows us to establish reliably that the spectrum asymmetry of the  $n = 21$  mode is due precisely to the presence of the second harmonic with a factor of three smaller amplitude.

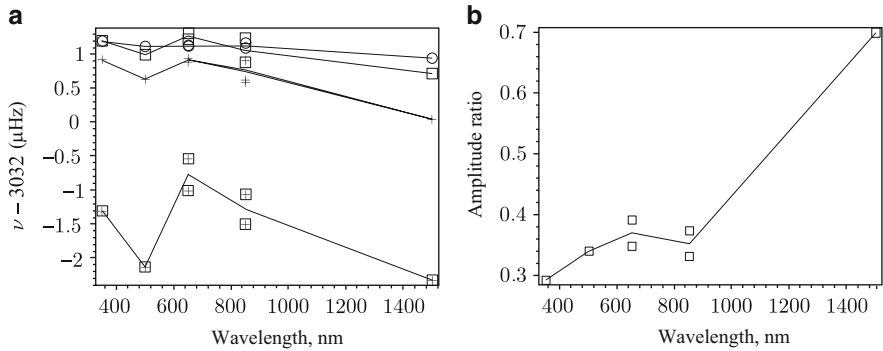


**Fig. 10** Panel **a**: crosses are the mean frequencies  $\overline{\omega(t)}$  and  $\tilde{\omega}$  of the  $n = 21$  mode before the harmonic separation, squares and crossed squares stand for the high- and low-frequency harmonics of the two-component signal, and circles indicate the frequencies corresponding to the maxima of the continuous oscillation spectra in each channel. Panel **b**: the harmonic amplitude ratio as a function of wavelength. From [14, p. 329]

The separation into components for the  $n = 21$  mode was performed for the brightness fluctuations in all optical channels of the DIFOS photometer. Not in all channels, the choice of the two-component signal was so ideal because of the slow, smooth frequency variations with time, which made the interaction of two modes differ from the ideal case of a two-component signal with constant harmonic amplitudes. As a result of slow variations of the instantaneous frequency, the maxima differ in height as seen, for example, in Fig. 7 (the lower middle panel). However, some uncertainty in choosing the height of the maxima turned out to have little effect on the frequencies and amplitudes of the components of the complex signal. Besides, a double maximum is sometimes observed suggesting the presence of a third component.

Figure 10 illustrates the results of harmonic separation for the  $n = 21$  mode for all optical channels of the DIFOS photometer. The squares in Fig. 10a denote the frequencies of the  $n = 21$  mode after the harmonic separation.

After the effect of the spurious harmonic has been removed, the  $n = 21$  mode frequencies turned out to be similar to those determined from the position of the spectral line maximum and denoted by circles in the figure. For comparison, the  $n = 21$  mode frequencies determined before the harmonic separation both by averaging the instantaneous frequency and by averaging over the spectrum are plotted in the same figure with crosses. The frequencies of the spurious harmonic indicated with crossed squares are seen to be, on average, lower than the  $n = 21$  mode frequency by  $3 \mu\text{Hz}$ . Figure 10b shows the ratio of the spurious harmonic amplitude to the amplitude of the  $n = 21$  mode. The relative amplitude of the spurious harmonic increases from 0.3 to 0.7 as we pass from the 350 nm to the 1,500 nm channel, which corresponds to the transition from the topmost to the deepest photospheric layers. Accordingly, the effect of the spurious harmonic on the frequency of the signal not separated into components increased with the increase of its amplitude.

The relationship between the mean frequency of the two-component signal  $\overline{\omega(t)}$  and the frequencies of its components  $\overline{\omega_1(t)}$ ,  $\overline{\omega_2(t)}$  is expressed by a simple formula

$$\overline{\omega(t)} = \frac{(\overline{A_1(t)})^2}{(\overline{A(t)})^2} \overline{\omega_1(t)} + \frac{(\overline{A_2(t)})^2}{(\overline{A(t)})^2} \overline{\omega_2(t)}, \quad (\overline{A(t)})^2 = (\overline{A_1(t)})^2 + (\overline{A_2(t)})^2. \quad (18)$$

The mean frequency of the two-component signal can be easily calculated from this equation using the harmonic separation scheme described above.

Thus, it was established that the difference between the  $n = 20$  and  $n = 21$  modes is associated with the effect of the spurious signal. After the latter was eliminated, the channel-to-channel variation of the  $n = 21$  mode frequency decreased significantly reaching approximately  $\pm 0.25 \mu\text{Hz}$ . However, this amplitude of the channel-to-channel frequency variation is twice the variation amplitude of the  $n = 20$  mode. This difference between the modes is due to the presence of another, higher-frequency spurious harmonic that distorts the  $n = 21$  mode spectrum. The presence of such harmonic is suggested by the double maxima of the instantaneous frequency. The effect of this harmonic on the  $n = 21$  mode frequency can also be eliminated, but we will not go into this problem here.

## Discussion of the $p$ -Mode Properties

The channel-to-channel phase variations revealed for the  $n = 20$  and  $n = 21$  modes suggest that phase shifts exist between the oscillations at different depths in the photosphere. This oscillation property could only be established on the basis of data from the DIFOS experiment—the only helioseismic experiment that allows the solar eigenmodes to be observed simultaneously in various bands of the continuous spectrum formed at all levels in the photosphere from the temperature minimum to the deepest layers where the  $\sim 1,500 \text{ nm}$  emission originates. The phase shift is the result of nonadiabatic nature of the oscillations. The 5-min oscillations in the photosphere are evanescent waves. The evanescent waves occur due to the total internal reflection in a medium in which the reflection takes place. In homogeneous media, they decrease exponentially with increasing distance from the boundary between the media where the reflection occurs. This is why they are called “evanescent.” In contrast to the homogeneous media, in a stratified solar atmosphere, in which the density decreases with height, the amplitude of evanescent waves increases with height as we move away from the site where the total internal reflection of the waves coming from the resonance layers under the photosphere takes place. However, the energy density of evanescent waves in the photosphere decreases rapidly with height.

The phase of nonadiabatic evanescent waves must remain constant; i.e., the evanescent waves can only propagate along the surface from which the total internal reflection takes place.

The phase shifts between the evanescent oscillations at different distances arise only if the oscillations are nonadiabatic. The cause of the phase shifts between the oscillations at different distances from the site of the total internal reflection and, accordingly, the appearance of traveling evanescent waves is the wave absorption due to the nonadiabaticity of oscillations.

The traveling waves transport energy to the places where the absorption is the fastest. In the photosphere, the efficiency of the radiative heat transfer responsible for the nonadiabaticity changes with depth. It is for this reason that the waves at different photospheric depths do not coincide in phase as revealed from DIFOS data. There are no other reasons that could lead to such effect. It should be noted that the theory of nonadiabatic waves in the photosphere encounters serious difficulties associated with the dependence of the radiative heat transfer on depth and the effect of temperature waves in the photosphere that interact with the  $p$ -modes [11–13].

A more detailed comparison of theory and observations requires both further development of the theory and analysis of the effect under discussion using a larger set of data from the DIFOS experiment.

As noted in introduction, despite the availability of very long-term observations, the accuracy of determining the oscillation frequencies corresponding to so long data series could not be achieved. This is explained by the jaggedness of the  $p$ -mode spectra. The method of analytical signal must help us resolve this problem, since it allows the separation of fluctuations of the amplitude and instantaneous frequency. The following procedure can be suggested. Comparing the amplitude and instantaneous frequency fluctuations, we can determine which of the amplitude fluctuations are associated with the spurious signals or with the signal splitting into components. These amplitude fluctuations are accompanied by frequency fluctuations. After that, the spurious signals and the additional components of the main signal can be singled out and eliminated (the latter procedure is not described in this section). After such signal cleaning, the jaggedness of the spectral line must disappear, and its width will correspond to the true line width of the  $p$ -modes. The accuracy of the frequency determination must increase accordingly and, in our opinion, it will be determined by frequency fluctuations alone rather than by the full half-width of the spectrum, which involves amplitude fluctuations.

The study of the  $p$ -mode properties described above has revealed a high stability of the oscillation frequency. The line broadening on account of frequency fluctuations turned out to be no more than  $0.4 \mu\text{Hz}$ , which corresponds to the relative stability of the oscillation frequency of  $10^{-4}$  or to a typical frequency variation timescale of the order of a month. This is in a certain conflict with the idea of stochastic excitation of oscillations, which is bound to lead to dephasing at every exciting “impact.” This must be reflected in short-term variations of the instantaneous frequency, since the latter is a time derivative of the phase. Besides, there must be fluctuations of the instantaneous amplitude synchronized with the dramatic changes in the instantaneous frequency.

The method of analytical signal seems to be perfectly suitable for studying the stochastic excitation of oscillations. However, nothing of the kind is observed in the above results. This is, probably, due to the fact that the characteristic timescale of

the stochastic fluctuations is of the order of 1 or 2 days. As a result, side frequencies must appear outside the main, central  $p$ -mode line. As emphasized repeatedly, the suggested method must be used to analyze long series of observation data, which will be done in the future.

The analytical signal concept described above differs from the method proposed by White and Cha [10] and applied later by Stebbins and Goode [7].

These authors found the analytical signal for the entire realization and not for a separate oscillation mode as we did. As a result, they determined the instantaneous frequency of the multi-component signal comprising all oscillation modes and the noise. Such a complex signal is, virtually, impossible to deal with. There are no methods for isolating the amplitudes and frequencies of individual modes from such a complex, multi-component analytical signal. Besides, because of an elementary mathematical error, the authors arrived at a conclusion that the purely amplitude modulation of the harmonic signal must be accompanied by the appearance of maxima of the instantaneous frequency. This is entirely in contradiction with the principle of separating the amplitude and frequency modulations.

## Dependence of the Oscillation Amplitude on the Observation Wavelength

One of the scientific problems that had to be approached in the course of the DIFOS experiment was the relationship between the  $p$ -mode amplitude and the observation wavelength. It is known that the solar radiation at different wavelengths originates at different subphotospheric levels, the 1,500 nm emission coming from the deepest layers.

The “amplitude–wavelength” relation was determined by two methods. The first one was as follows. We plotted the oscillation spectra for each of the spectral bands. The length of the data set was chosen such that it did not exceed the  $p$ -mode characteristic lifetime (from 3 to 10 days) but was sufficient for the individual  $p$ -modes to be reliably resolved and identified. The optimal length of the data set was, in our opinion, about 2 days, which corresponded to 30 orbital revolutions of the satellite. In order to increase the signal-to-noise ratio, we summed up these 2-day spectra over a sufficiently long time interval. An example of such summary spectrum for one of the observation channels is represented in Fig. 11.

The amplitudes of about ten reliably identified  $p$ -modes, the same for all observation channels, were derived from the spectra for each spectral band, and the results obtained were used to plot the “amplitude–wavelength” relation.

In the second method, the amplitude spectra were plotted using the time series corresponding to each particular orbital revolution. These spectra were summed up for the same time interval as in the first method. In this case, the individual oscillation modes could not be resolved, but the envelope of the 5-min oscillation spectrum was obtained for each observation band (Fig. 12).

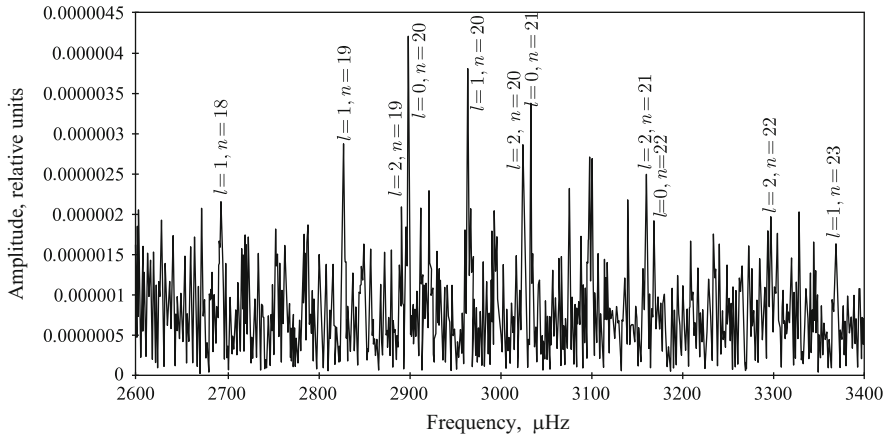


**Fig. 11** Amplitude spectrum of the 5-min solar oscillations in the 650 nm spectral band based on the 2-day series of CORONAS-F/DIFOS data (orbits 1831–1920, 144 h, 29 November to 5 December 2001). From [5, pp. 871–875]

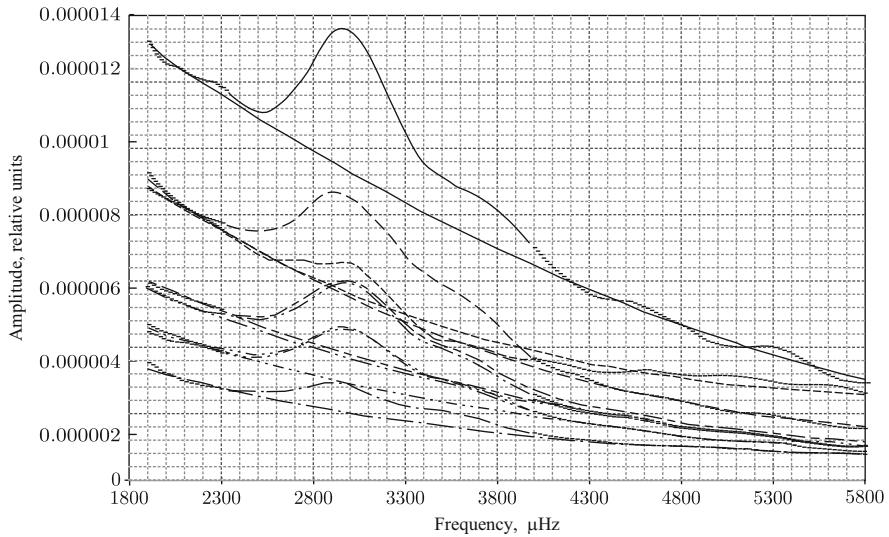


**Fig. 12** Amplitude spectrum of the 5-min solar oscillations based on the series of one-revolution CORONAS-F/DIFOS data (orbital revolutions 1831–1920, 29 November to 5 December 2001). The fitting curves for the noise component are presented

The “amplitude–wavelength” relation was plotted using the amplitude ratios that correspond to the maximum of the spectrum envelope (3,000  $\mu\text{Hz}$ ).

The plots obtained by both methods are shown in Fig. 13.

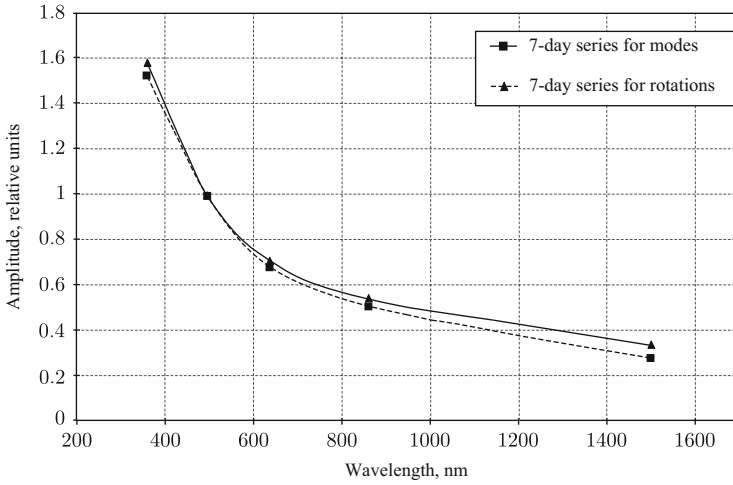


**Fig. 13** The  $p$ -mode amplitudes vs. the observation wavelength for individual oscillation modes and for the spectrum envelope

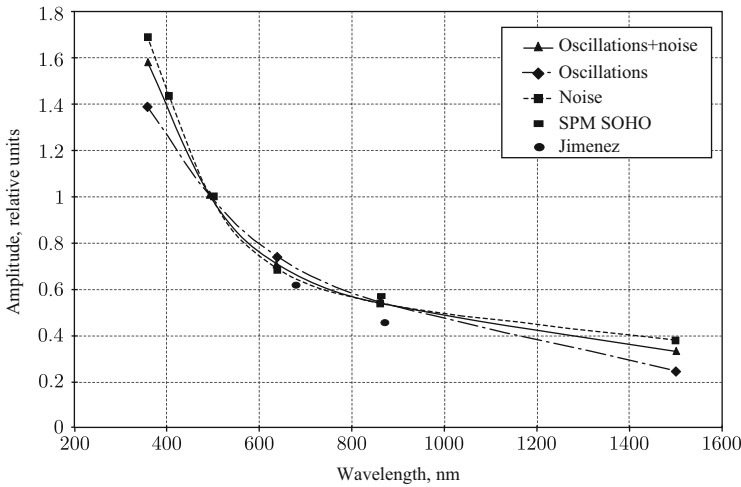


**Fig. 14** The amplitude of  $p$ -modes, solar noise, and total signal (oscillations + noise) as a function of the observation wavelength

One can see that the two curves agree perfectly well. A minor difference in the long-wave range is, apparently, due to the fact that the first method was applied to the range of 2,500–3,500  $\mu\text{Hz}$  and the second one, only to 3,000  $\mu\text{Hz}$ .

The spectral curves in Fig. 12 show that the  $p$ -mode amplitude can be separated from the solar noise by approximating the noise component to the 5-min oscillation range and, then, subtracting it from the total signal. The result of such calculation is represented in Fig. 14.



To interpret the results obtained, we need a theory of solar brightness fluctuations under the effect of the  $p$ -modes. It is necessary to find out how the oscillation amplitude and phase depend on the wavelength band the fluctuations are measured in.

Since the brightness fluctuations caused by the  $p$ -modes have small amplitudes, we can use the linear approximation and expand the expression for the solar radiation flux into minor disturbances of temperature and density. This yields the following expression for the brightness fluctuations at a frequency  $\nu$ :

$$\begin{aligned} \delta F_\nu = & \int_0^\infty \frac{dB_\nu(\tau_\nu)}{d \ln T} \frac{\delta T(\tau_\nu)}{T_0(\tau_\nu)} E_2(\tau_\nu) d\tau_\nu \\ & - \int_0^\infty \left( \frac{\partial \ln \chi_\nu(\tau_\nu)}{\partial \ln T} \right)_\rho \frac{\delta T(\tau_\nu)}{T_0(\tau_\nu)} \int_{\tau_\nu}^\infty \frac{dB_\nu(\tau'_\nu)}{d\tau'_\nu} E_2(\tau'_\nu) d\tau'_\nu d\tau_\nu \\ & - \int_0^\infty \left( \frac{\partial \ln \chi_\nu(\tau_\nu)}{\partial \ln \rho} \right)_T \frac{\delta \rho(\tau_\nu)}{\rho_0(\tau_\nu)} \int_{\tau_\nu}^\infty \frac{dB_\nu(\tau'_\nu)}{d\tau'_\nu} E_2(\tau'_\nu) d\tau'_\nu d\tau_\nu, \end{aligned} \quad (19)$$

where  $\tau_\nu$  is the optical depth at the frequency  $\nu$ ,  $B_\nu(\tau_\nu)$  is the Planck function as a function of optical depth,  $E_2(\tau_\nu)$  is the integral exponential function,  $\chi_\nu(\tau_\nu)$  is the absorption coefficient at a given frequency,  $\delta T$  and  $\delta \rho$  are the temperature and density fluctuations caused, in our case, by the  $p$ -modes, and  $T_0$  and  $\rho_0$  are the undisturbed temperature and density values at a given optical depth.

This formula takes into account two effects responsible for fluctuations of the solar radiation at a given frequency. The first integral in the formula accounts for the temperature dependence of the Planck function and appears as a result of expansion of the latter into minor temperature disturbances with allowance for the linear term alone. The other terms appear because the absorption coefficient depends on both temperature and density. In the linear approximation, this can be expressed as:

$$\delta \chi_\nu = \left( \frac{\partial \chi_\nu}{\partial T} \right)_\rho \delta T + \left( \frac{\partial \chi_\nu}{\partial \rho} \right)_T \delta \rho. \quad (20)$$

If the absorption coefficient increases as a result of temperature and density fluctuations, the flux emerging from the photosphere decreases and vice versa. In order to simplify the general formula, we assumed that the  $p$ -modes do not differ significantly from adiabatic oscillations. In this case, the density fluctuations are expressed in terms of the temperature fluctuations as follows:

$$\frac{\delta \rho}{\rho_0} = \frac{\delta T}{(\gamma - 1)T_0}. \quad (21)$$

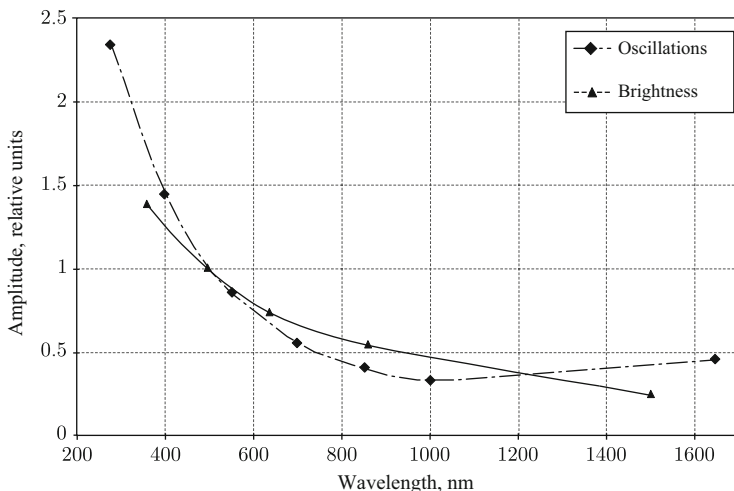


**Fig. 15** The dependence of the  $p$ -mode amplitude and the theoretical dependence of the solar brightness fluctuations on the observation wavelength

Using this formula, we can obtain an expression for the solar brightness, which depends only on brightness fluctuations. However, to calculate this integral expression, we need to know how the temperature fluctuations depend on depth. It may be assumed that  $\delta T/T_0 = \text{const}$ , i.e., is independent of depth. In this special case, we can remove  $\delta T/T_0$  from under the integral sign and perform integration. Such calculations were made using the photosphere models [15]. The results are represented in Fig. 15.

A certain discrepancy between the theory and observations may be due to the assumption of nonadiabaticity of oscillations and  $\delta T/T_0 = \text{const}$ , as well as to the use of the mean inhomogeneous atmosphere model that takes no account of the granulation.

## References

1. Boashash, B.: Time–Frequency Signals Analysis: Methods and Applications. Wiley, New York (1992)
2. Fink, L.M.: Probl. Inf. Transf. **2**(4), 26 (1966) (in Russian)
3. Fink, L.M.: Signals, Noise, and Errors. Radio and Communications, Moscow (1984) (in Russian)
4. Gabor, D.J.: Inst. Electr. Eng. **46**(26), 429 (1946)
5. Lebedev, N.I., Kuznetsov, V.D., et al.: The helioseismological CORONAS-F DIFOS experiment. Astron. Rep. **48**(10), 871–875 (2004)
6. Rylov, S.M.: Trudy FIAN (Proc. Lebedev Phys. Inst.) **11**(1), 43 (1940) (in Russian)
7. Stebbins, R., Goode, P.R.: Waves in solar photosphere. Sol. Phys. **110**, 237 (1987)

8. Vainshtein, L.A., Vakman, D.E.: Frequency Separation in the Oscillation and Wave Theory. Nauka, Moscow (1983) (in Russian)
9. Vakman, D.E., Vainshtein, L.A.: Amplitude, phase, frequency-fundamental concepts of oscillation theory. *Sov. Phys.—Usp.* **20**(12), 1002–1016 (1977)
10. White, O.R., Cha, M.Y.: Analysis of the 5 min oscillatory photospheric motions. *Sol. Phys.* **31**, 23 (1973)
11. Zhugzhda, Yu.D.: Nonadiabatic oscillations in an isothermal atmosphere. *Pisma v AZh.* **9**, 631 (1983a) (in Russian)
12. Zhugzhda, Yu.D.: Non-adiabatic oscillations in an isothermal atmosphere. *Astrophys. Space Sci.* **95**(2), L255 (1983b)
13. Zhugzhda, Y.D.: Temperature waves in the solar photosphere. *Sol. Phys.* **124**, 205 (1989)
14. Zhugzhda, Yu.D.: Analytical signal as a tool for studying the solar  $p$ -mode properties. *Astron. Lett.* **32**(5), 329 (2006)
15. Zhugzhda, Y.D., Staude, J., Bartling, G.: Spectral darkening functions of solar  $p$ -modes—an effective tool for helioseismology. *Astron. Astrophys.* **305**, L33–L36 (1996)

The Coronas-F Space Mission

Key Results for Solar Terrestrial Physics

Kuznetsov, V.D. (Ed.)

2014, XII, 483 p. 319 illus., 48 illus. in color., Hardcover

ISBN: 978-3-642-39267-2